Localization and segmentation of optic disc in retinal images using Circular Hough transform and Grow Cut algorithm

Muhammad Abdullah, Muhammad Moazam Fraz, Sarah A Barman

Automated retinal image analysis has been emerging as an important diagnostic tool for early detection of eye related disease such as glaucoma and diabetic retinopathy. In this paper, we have presented a robust methodology for optic disc detection and boundary segmentation, which can be seen as the preliminary step in the development of a computer-assisted diagnostic system for glaucoma in retinal images. The proposed method is based on morphological operations, Circular Hough transform and Grow Cut algorithm. The morphological operators are used to enhance the optic disc and remove the retinal vasculature and other pathologies. The optic disc center is approximated using the Circular Hough Transform, and the Grow Cut algorithm is employed to precisely segment the optic disc boundary. The method is quantitatively evaluated on five publicly available retinal image databases DRIVE, DIARETDB1, CHASE_DB1, DRIONS-DB, Messidor and one local Shifa Hospital Database. The method achieves optic disc detection success rate as 100% for these databases with the exception of 99.09% and 99.25% for the DRIONS-DB, Messidor, and ONHSD databases respectively. The optic disc boundary detection achieved an average spatial overlap of 78.6%, 85.12%, 83.23%, 85.1%, 87.93%, 80.1%, and 86.1% respectively for these databases. This unique method has shown significant improvement over existing methods in terms of detection and boundary extraction of the optic disc.

1 # Localization and Segmentation of Optic Disc in Retinal Images using
2 ## Circular Hough Transform and Grow Cut Algorithm

4 Muhammad Abdullah[1], Muhammad Moazam Fraz[2] and Sarah A. Barman[3]

5 *[1] School of Electrical Engineering and Computer Science, National University of Sciences and*

6 *Technology, Sector H-12, Islamabad, 44000, Pakistan.*

7 *[2] Faculty of Science Engineering and Computing, Kingston University London, United Kingdom*

9 Corresponding Author:

10   Muhammad Moazam Fraz

11 Street Address:

12   School of Electrical Engineering and Computer Science, National University of Sciences

13   and Technology, Sector H-12, Islamabad, 44000, Pakistan.

15 Email Address:

16   moazam.fraz@seecs.edu.pk

18 Phone:

19   00 92 51 9085 2179

Abstract

22 Automated retinal image analysis has been emerging as an important diagnostic tool for early
23 detection of eye related disease such as glaucoma and diabetic retinopathy. In this paper, we
24 have presented a robust methodology for optic disc detection and boundary segmentation, which
25 can be seen as the preliminary step in the development of a computer-assisted diagnostic system
26 for glaucoma in retinal images. The proposed method is based on morphological operations,
27 Circular Hough transform and Grow Cut algorithm. The morphological operators are used to
28 enhance the optic disc and remove the retinal vasculature and other pathologies. The optic disc
29 center is approximated using the Circular Hough Transform, and the Grow Cut algorithm is
30 employed to precisely segment the optic disc boundary. The method is quantitatively evaluated
31 on five publicly available retinal image databases DRIVE, DIARETDB1, CHASE_DB1,
32 DRIONS-DB, Messidor and one local Shifa Hospital Database. The method achieves optic disc
33 detection success rate as 100% for these databases with the exception of 99.09% and 99.25% for
34 the DRIONS-DB, Messidor, and ONHSD databases respectively. The optic disc boundary
35 detection achieved an average spatial overlap of 78.6%, 85.12%, 83.23%, 85.1%, 87.93%,
36 80.1%, and 86.1% respectively for these databases. This unique method has shown significant
37 improvement over existing methods in terms of detection and boundary extraction of the optic
38 disc.

1. Introduction

40 Digital retinal images are widely used for early detection of retinal, ophthalmic and systemic
41 diseases because they provide a non-invasive window to the human circularity system and
42 associated pathologies (Jack J. Kanski & Brad Bowling 2015). Glaucoma and Diabetic
43 Retinopathy (DR) are among major retinal disease which are the leading cause of vision loss and
44 blindness in the working population (Federation 2013). Early detection of these disease by
45 screening programs and subsequent treatment can prevent blindness. Computer aided diagnostic
46 retinal image analysis is the first step in automated screening of these diseases in large
47 population based studies (Fraz et al. 2015). The change in anatomical structures in human retina,
48 which includes retinal vasculature, Optic Disc (OD), optic cup and retinal pathologies are the
49 early diagnostic indicators of several diseases such as DR, Macula Edema and Glaucoma (Jack J.
50 Kanski & Brad Bowling 2015). Among these, the OD is the most important feature because its
51 visual aspects are central for glaucoma detection and other lesions assessment related to DR. The
52 important anatomical structures presented in the retinal image are shown in Figure 1. OD
53 detection is preliminary step for glaucoma screening, which is globally the second leading cause
54 of blindness. Moreover, it helps in the detection and localization of other retinal structures which
55 includes the fovea, macula and estimating vascular changes (Basit & Fraz 2015).

56
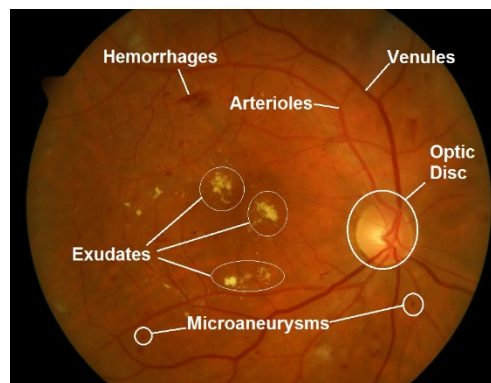
57 **Figure 1 Important features in retinal fundus image.**

58 Glaucoma is caused by the increase in the intraocular fluid pressure in the Optic Nerve Head
59 (ONH), because of either blockage or a higher production of aqueous humor of the eye (Jack J.
60 Kanski & Brad Bowling 2015). Glaucoma remains asymptomatic at an early stage and slowly
61 progress with time which ultimately leads to blindness. Medical treatment is only effective at the
62 early stages because the optic nerve, once damaged can't be cured (Weinreb et al. 2014). The
63 early prevalence of Glaucoma can be identified by localization and segmentation of the OD and
64 Optic Cup, followed by computing the cup-to-disc ratio. The structural changes in OD furnish
65 critical clues pertaining to glaucoma prognosis (Abramoff et al. 2010). A Computer Assisted
66 Diagnosis (CAD) system is necessary for large population based screening of Glaucoma. OD
67 localization and segmentation is the first step towards the development of CAD. Knowing the
68 significance such systems, several OD approaches have been proposed and attempted by many
69 but it's still an active research area.
70 The OD appears as a variable sized, bright yellowish region, slightly oval in shape with blood
71 vessels converging towards its center. These features are mostly used for automated OD
72 localization. Retinal pathologies like exudates and lesions, if present, may appear like the shape
73 of a disc, thus may cause false detection (Basit & Fraz 2015). In CAD, accurate detection and
74 segmentation of the OD is quite a challenging task because of various factors like boundary
75 artifacts, missing edges and poor textural contrast. The variation in illumination conditions,
76 luminosity and contrast during image acquisition are added challenges (Haleem et al. 2013).
77 Moreover, the OD boundary is not constant because of the presence of incoming blood vessels
78 which produce a fused boundary. Another distractor is papillary atrophy which, if present,
79 appears as the bright region outside the OD and thus deforms the OD boundary (Aquino et al.
80 2010).
81 This paper presents a new approach for automatic detection and segmentation of the OD based
82 on morphological operations, Circular Hough Transform (CHT) (Illingworth & Kittler 1987) and
83 Grow Cut (GC) algorithm (Vezhnevets & Konouchine 2005). The GC algorithm has been widely
84 used in many application areas of image segmentation, but has not been applied within the
85 framework of retinal image analysis. To the limit of our knowledge, the GC algorithm has been
86 utilized for the first time in localizing and segmenting the OD in retinal images. The method is
87 evaluated on six retinal image datasets exhibiting different morphological characteristics.
88 Experimental evaluation shows that this method is computationally fast in processing, robust to
89 the variation in image contrast, illumination and presence of pathologies; and comparable with
90 the state-of-the-art methodologies in terms of quantitative performance metrics.
91 It's worth mentioning that this work is aimed at contributing to the development of automatic
92 systems for glaucoma detection that are currently under development. Although other published

93   solutions can be used, this work presents higher accuracy, robustness and is tolerant to a vast
94   variety of image characteristics, which make it suitable for integration with a glaucoma detection
95   system.
96   The organization of the paper is as follows. Section 2 presents a comprehensive overview of the
97   OD localization and segmentation methodologies available in the literature. Section 3 explains
98   the proposed methodology in detail. The materials and the performance metrics used to evaluate
99   the proposed methodology are illustrated in section 4. The results and comparison with other
100 methods are given in section 5. The paper is concluded in section 6.

1   Related Work

102 A significant number of papers have been published to deal with the OD detection and
103 segmentation (Haleem et al. 2013). Some papers only perform OD detection while others
104 perform both detection and segmentation. Here we briefly discuss both of the groups.

1.1   Methods for OD detection

106 Hoover and Goldbaum (Hoover & Goldbaum 2003) use vascular origin to detect the OD center.
107 To detect the vascular convergence point they use a fuzzy convergence and voting type
108 algorithm. Niemeijer et al. (Niemeijer et al. 2009) performed vascular segmentation and measure
109 the distance at specific locations with the help of a kNN regressor. The point with lowest
110 distance to the OD is selected as the OD center. Inspired by results from vascular direction
111 methods, Youssif et al. (Youssif et al. 2008) used a matched filter to match the direction of blood
112 vessels around the OD area and a vessel direction map is obtained by segmenting vessels.
113 Mendonca et al.(Mendonca et al. 2013) further improve the results by using the entropy of
114 vascular direction to assess the convergence point of vessels. To increase robustness, they
115 constrain the search for maximal entropy to the areas with high intensities. In (Lu 2011), a
116 circular transformation is used to capture a circular shape OD and evaluate image variation along
117 multiple radial lines. Pixels with maximum variations are determined, as they can be further used
118 for OD center and boundary localization. Another methodology based on the Radon
119 transformation of overlapping window (Pourreza-Shahri et al. 2014) has achieved 100% success
120 in DRIVE and 96.3% on STARE databases.

1.2   Methods for OD detection and boundary segmentation

122 In (Welfer et al. 2010), a method based on mathematical morphology is proposed to detect and
123 segment the OD in images from DRIVE and DIARETDB1. This work is extended in (Welfer et
124 al. 2013) by incorporating a multiscale morphologic approach. Marin et al. (Marin et al. 2015)
125 proposed a two step automatic thresholding on a morphologically processed bright enhanced
126 region to get a reduced region of interest, followed by the application of Circular Hough
127 Transformation (CHT) to get the OD center and OD region. Seo et al. (Seo et al. 2004) also use
128 morphological and Canny edge detection filters to segment and detect the OD rim.
129 Kande et al. (Kande et al. 2008) detected the OD by using maximum local variance with 92.53%
130 success rate and geometric Active Contour Model (ACM) for OD segmentation. In (Aquino et al.
131 2010), a template based approach is used for OD segmentation. They applied morphological and
132 edge detection techniques followed by CHT to approximate circular objects. Lupascu et al.
133 (Lupascu et al. 2008) used a regression method and texture descriptors for circular OD fitting.
134 An approach based on Principal Component Analysis and mathematical modelling is presented
135 in (Morales et al. 2013), which utilizes a generalized distance function, stochastic watershed and
136 geodesic transformations. The result is finally approximated by a circular approximation. Walter
137 et al. (Walter et al. 2002) presents a methodology based on Watershed transformation and

138   morphological processing. In (Hsiao et al. 2012), illumination correction technique was used to
139   detect optic disc. They select high intensity pixels as candidates for OD and among those
140   candidate pixels they select OD pixel as one with the highest variance. For segmentation, the
141   Supervised Gradient Vector Flow (SGVF) snake model is used. By extending the SGVF snake in
142   each iteration, contour points get updated and classified based on features. Statistical information
143   and features extracted from trained images were then used for classification. In (Joshi et al.
144   2011), the Chan-Vese model has been extended by introducing image information around a
145   contour point. Inspired by the work proposed in (Joshi et al. 2011), the local binary fitting
146   energy ACM (Mittapalli & Kande 2016) is proposed to integrate the local image information
147   which includes texture color and intensity for each point of interest. A multi-resolution Sliding
148   Band Filter (SBF) was used in (Dashtbozorg et al. 2015) for OD segmentation. Super-pixels are
149   employed in (Cheng et al. 2013) such that each super-pixel is classified as OD or non-OD. It has
150   been observed that the confluence of vessels in the OD region affects the precision of OD
151   segmentation methods. However, to overcome the influence of the presence of vessels some
152   methods try to eliminate them from image. In this paper, we propose a new approach for
153   automatic OD detection and segmentation which is not influenced by the confluence of vessels in
154   OD area, therefore, no template or vessel map is required in advance.

155   2   The Methodology

156   This work presents an OD detection and segmentation methodology which is able to detect the
157   OD center without using any template or prior vascular information, an extension to our earlier
158   work (Abdullah & Fraz 2015). The OD appears as a yellowish structure in retinal fundus images
159   with shape varying from circular to slightly elliptical and has the highest intensity value pixels.
160   However, the presence of brightness artifacts can make the OD merge into the background and
161   lose its brightness. Furthermore, the presence of several pathological structures such as exudates
162   may take the shape of the OD and may have the highest intensity value. The proposed algorithm
163   is based on morphological operations, Circular Hough transform and Grow Cut algorithm. The
164   morphological operators are used to enhance the optic disc and remove the retinal vasculature
165   and other pathologies. The optic disc center is approximated using the Circular Hough
166   Transform, and the Grow Cut algorithm is employed to precisely segment the optic disc
167   boundary.

168   2.1   Preprocessing

169   The variation in image contrast, background illumination and pigmentation is normalized by
170   applying pre-processing operations to the retinal images.
171   The green channel of an RGB image gives maximum contrast between exudates and the
172   neighboring regions (Fraz et al. 2012b). Therefore, the green channel of RGB images is
173   processed for normalization of contrast and luminosity. A variety of algorithms for contrast and
174   luminosity normalization in retinal images are available in the literature, and these
175   methodologies are either based on subtracting the estimated background from the original image
176   (Fraz et al. 2014) or on dividing the later by the former (Foracchia et al. 2005; Vázquez et al.
177   2013). However, our earlier work (Fraz et al. 2014) shows that the results of both methods are
178   similar with no appreciable advantage of one over the other. We have used the subtractive
179   method as it has been reported in our earlier work (Fraz et al. 2014). The background pixel
180   intensities are estimated and the difference between the estimated background and the green
181   channel is computed to produce the normalized image. The background of the retinal image,
182   denoted as "Ibg" is estimated by applying a filtering operation with an arithmetic mean kernel.

183 The size of the filter kernel is not a critical parameter as long as it is large enough to ensure the
184 blurred image contains no visible structures such as optic disc, exudates or blood vessels. In this
185 work, we have used an 89 × 89 pixel kernel. The difference between the estimated background
186 "Ibg" and the morphologically opened image "Iopen" is calculated on pixel basis. Thus the
187 background normalized image "Inorm" is obtained using:

188
$$I_{norm}(x, y) = I_{open}(x, y) - I_{bg}(x, y) \tag{1}$$

189 Due to different illumination conditions in the acquisition process, there may be significant
190 intensity variations between images. These intensity variations make it difficult to use the best
191 possible technique for all of the images, thus shade corrections were necessary and have been
192 applied. A global linear transformation function is applied to modify the pixel intensities.

193
$$I_{SC}(x,y) = \begin{cases} 0 & if\ I_{norm}(x,y) < 0 \\ 1 & if\ I_{norm}(x,y) > 1 \\ I_{adjusted}(x,y) & otherwise \end{cases} \tag{2}$$

194
$$I_{adjusted}(x, y) = I_{norm}(x, y) - IntVal_{MaxPixels} + 0.5 \tag{3}$$

195 Where $I_{sc}(x, y)$ is the shade corrected image, $I_{norm}(x, y)$ is the background normalized image,
196 $IntVal_{MostPixels}$ is the intensity value representing the most number of pixels in the normalized image
197 $I_{norm}(x, y)$. Pixels with this intensity value $IntVal_{MostPixels}$ represent the background (Fraz et al.
198 2012a). This global transformation function normalizes or shade corrects the image by setting the
199 background pixels to 0.5, which can be observed in Figure 2(c).

2.2 Optic Disc Detection

201 After pre-processing, the OD appears as the brightest structure in the image with varying size
202 and appearance. The retinal blood vessels originate from the OD and branch out to spread in the
203 retinal image. A morphological closing operation with a disc shaped structuring element is
204 applied to the pre-processed image in order to remove the vasculature from the image. The result
205 is shown in Figure 2(d).
206 CHT, an extension of Hough transform (HT) (Hough 1962), is for the detection of circular
207 objects from the image. For the detection of a circle, the HT is based on the equation of circle,
208 defined as

209
$$(x_i - a)^2 + (y_i - b)^2 = r^2 \tag{4}$$

210 Where, "(a, b)" represents the coordinates of the center of the circle and "r" denotes the radius.
211 In order to increase the performance of CHT we resize all images to a common resolution and
212 search for the bright circles with an experimented selected radius range of 29 to 50 pixels. To
213 avoid false detection of OD we optimized our system by applying CHT on each image at
214 different sensitivity levels and among circular responses generated by CHT we take only strong
215 circle. Strong circles are the ones that correspond to the OD while the rest are either exudates or
216 misleading regions. The results of intermediary processing steps for OD localization/detection
217 are shown in Figure 2.
218

2.3 Optic Disc Segmentation

In the preprocessed image, the OD area is treated as foreground (fg) and the rest of the retinal image is considered as background (bg). The Grow Cut (GC) (Vezhnevets & Konouchine 2005) algorithm separates the fg from bg using the von Neumann Neighborhood principle (Toffoli & Margolus 1987) and seeded region growing. The detected OD center is chosen as initial seed points for fg area whereas the bg seed points are automatically chosen from rest of image. This algorithm iteratively checks each neighboring pixel and decides its region-wise membership. The GC algorithm use cellular automata for image modelling. Each image pixel "p" can be represented by a triplet (lp, θp, Cp). Where, "lp" represents the class label of the pixel "p" to which it belongs, "θp" represents the "strength" of the pixel "p" which is a measure of the certainty of the pixel "p" that should be labelled as "lp". The label of a pixel whose "strength" = 1 cannot be changed during the algorithm progress, whereas the pixel label whose "strength" < 1 may change during algorithm execution. "Cp" represents the pixel greyscale value.

(a)   (b)   (c)

(d)   (e)   (f)
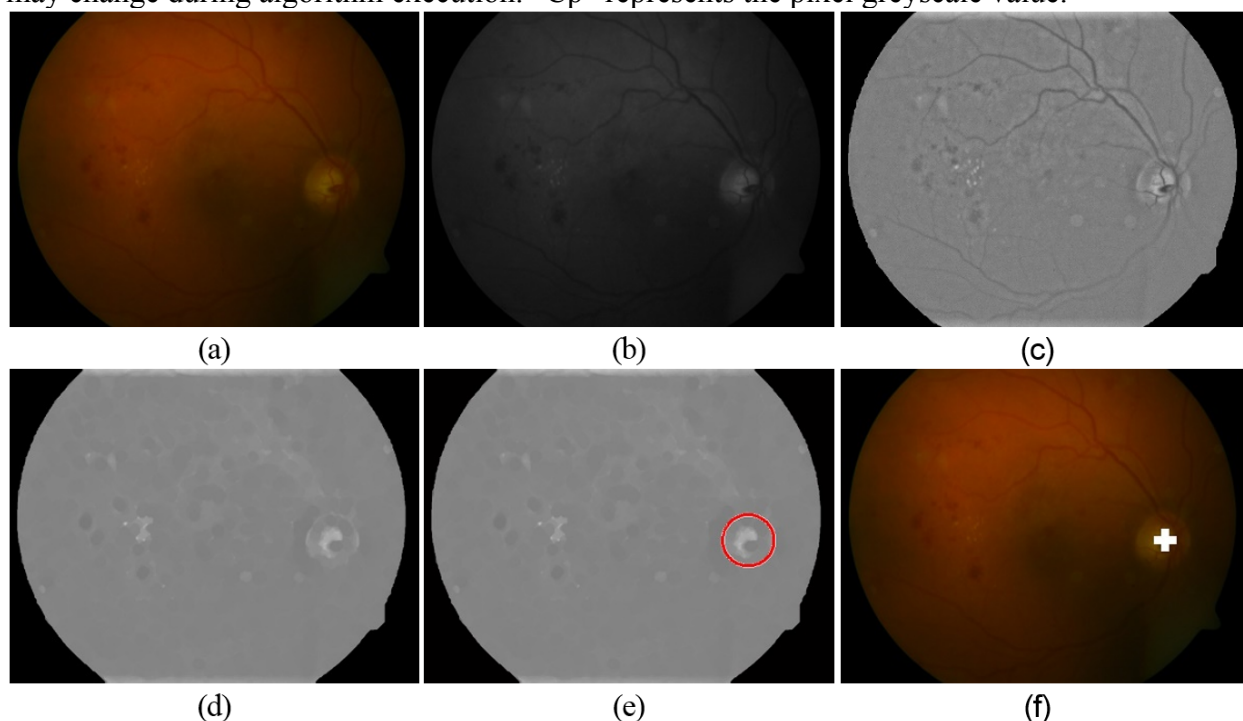
Figure 2 Processing steps for OD detection.
(a) RGB retinal image (b) Green Channel image (c) Preprocessed green channel image (d) Blood vessel removed image (e) Circular approximation of optic disc by CHT (f) Detected OD center

At the initial stage of the algorithm, the triplet for all pixels are set as,

$$l_p = 0, \ \theta_p = 0, \ C_p = RGB_p \qquad (5)$$

Which means that initially all pixels have undefined labels and zero strength. The aim of the GC algorithm in segmenting the OD is to assign a label to each pixel in the image regarding whether it belongs to OD or to the retinal image background. To start the algorithm, we initialized seeds by setting labels for the optic disc (+1) and non-OD (-1). Once the seeds are initialized, the process keeps on iteratively assigning labels to each pixel in the image until all pixels are labelled. For each pixel p and its neighbors xi (i=1 to 8), quantity "g" is computed which is monotonous decreasing function where g (xi) ∈ [0, 1] such that

245
$$g(x_i) = \frac{\|C_p - C_{xi}\|_2}{max \, \|C\|_2} \qquad (6)$$

246 As we were using green channel of the image so $\|C_p - C_{xi}\|$ is equal to $\|I_p - I_{x_i}\|$, where I_p and I_{x_i}

247 are the intensities of pixels p and xi respectively. $max\,\|C\|_2$ is equal to 2L -1, where L is the bit

248 depth of the image. Afterwards, the algorithm iteratively compute λ (xi) for all pixels xi which

249 don't have label "undefined" such that:

250
$$\lambda(x_i) = g(x_i) . \theta(x_i) \qquad (7)$$

251 If $\lambda(x_i) > \theta_p$ then a pixel takes the label and strength of xi otherwise it keeps its own label and

252 "strength". The algorithm terminates when all the pixels are labeled and the pixel label stops

253 changing. In the end, the segmented OD boundary is approximated to an elliptical shape by using

254 ellipse equation which involves drawing of ellipse outline over the segmented boundary of GC.

255 The processing steps of OD boundary extraction are shown in Figure 3. The circular

256 approximation of the OD boundary is illustrated in Figure 4.

257

(a)   (b)   (c)   (d)
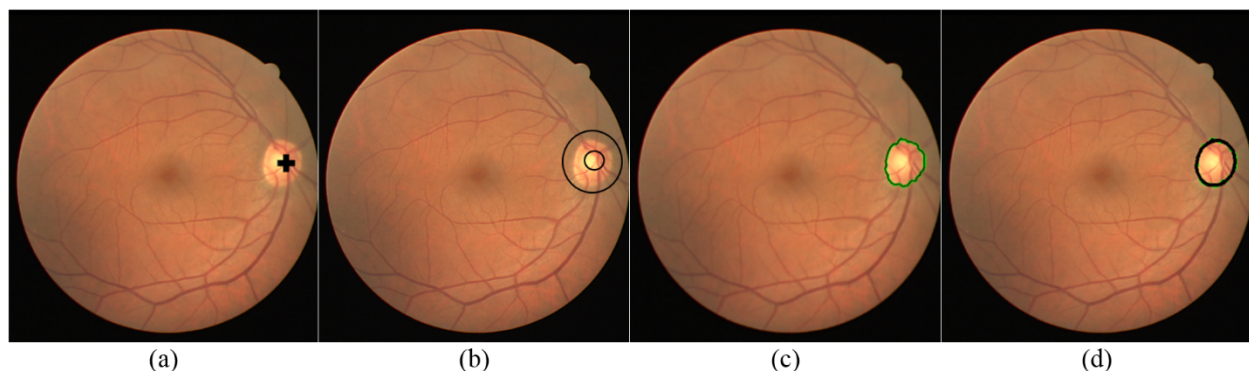
258
259 **Figure 3 Steps for OD boundary extraction**

260 (A) Original RGB image with detected central point of optic disc, (B) Foreground (optic disc area represented by

261 small circle) selection points and background (non-optic disc region represented by large circle) selection points (C)

262 Result of Grow Cut for boundary segmentation, (D) Boundary approximation (in black) of grow cut.

(a)   (b)
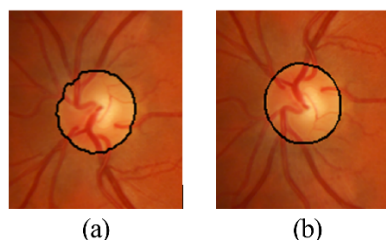
263
264 **Figure 4 Close up view of (a) Grow Cut segmentation; (b) approximation of Grow Cut.**

3   Materials

266 The proposed methodology is evaluated on five publicly available retinal image databases and

267 one local database.

3.1 DRIVE

DRIVE (2004) is a publically available database consisting of 40 images with resolution 584 × 565 pixels. Out of these 40 images, 7 are pathological, containing pigment epithelium changes, exudates and hemorrhages.

3.2 DIARETDB1

The DIARETDB1 (Kauppi et al. 2007) database comprised 89 fundus images which are obtained with a 50° of FOV using a fundus camera and are in PNG format. These images are of size 1500 × 1152 pixels, with 24bits/pixel.

3.3 CHASEDB1

The CHASEDB1 (Fraz et al. 2012c) database consists of 28 images captured from a Nidek NM 200D camera at 30° FOV. Images are of 1280 × 960 pixels resolution, which are affected by illumination artifacts and poor contrast.

3.4 DRIONS-DB

The DRIONS (Carmona et al. 2008) database consists of 110 images of 600 × 400 resolution, with 8 bits/pixel. In these 110 images, 50 images contain some sort of defect, such as illumination artifacts, rim blurredness and papillary atrophy, which may hinder the detection and segmentation problem.

3.5 Messidor

The Messidor (Decenciere et al. 2014) database consists of 1200 retinal fundus images which were captured from 3CCD color video camera on Topcon TRC NW6 non-mydriatic retinograph, with 45° of FOV.

3.6 ONHSD

The ONHSD (Lowell et al. 2004) database consists of 99 fundus images of 640 × 480 resolution. Images were captured from canon CR6 45MNf camera with 45° of FOV. Images were acquired from 50 patients, 19 out of which were diabetic.

3.7 Shifa Database

This database belongs to Department of Ophthalmology, Shifa International Hospital Islamabad, Pakistan. 19 images are healthy while the rest of them have some sort pathological symptoms and illumination artifacts. The dataset consists of 111 fundus images of 1936 × 1296 resolution, acquired with a 45° field of view.

3.8 Ground Truths

The OD in all the images from the above mentioned databases is hand labelled by ophthalmic experts from the Armed Forces Institute of Ophthalmology, Rawalpindi, Pakistan and used as ground truths. For 1200 images in the Messidor database, we have used the ground truths provided by Aquino et.al (Aquino et al. 2010). The quantitative results are based on comparison of automatic segmented images with these ground truths.

3.9 Quantitative Performance Measures

The outcome of OD detection and the segmentation process results in the classification of pixels belong to OD region or non-OD region. There are four possibilities for pixel classification, illustrated in Table 1, True Positive (TP), True Negative (TN), False Positive (FP) and false Negative (FN). The first two are the result of mutual agreement between predicted values and actual values while the last two are the result of the wrong prediction. TP is the case when the system predicts the pixel belongs to the OD and is actually an OD pixel in reference to the ground truth image, while in the case of TN both the system and actual ground truth identify a

312 pixel as a non-OD pixel. FP is the case where the system predicts the pixel as an OD pixel when
313 it actually belongs to non-OD region in ground truth, whereas, in the FN case the system predicts
314 a pixel as a non-OD pixel when it actually is an OD pixel.
315 The metrics used to evaluate the quantitative performance of the proposed methodology are
316 given in Table 2. We used Sensitivity (SN), Specificity (SP), Accuracy (Acc), Positive Predicted
317 Value (PPV), False Discovery Rate (FDR) and Overlap. The overlap metric is defined in (8).

318
$$Overlap = \frac{Area(ground\ truth \cap predicted)}{Area(ground\ truth \cup predicted)} \qquad (8)$$

319 Moreover, we have used the DICE similarity index to measure the similarity between the
320 segmented optic disc and the ground truth. The DICE index is a measurement of spatial overlap
321 used widely for comparing segmentation results, with a value ranging from 0 to 1. The DICE
322 coefficient can be defined as two times the volume of the intersection between two
323 segmentations divided by the sum of the volumes of the two segmentations, which is represented
324 in (9).

325
$$DICE = \frac{2 * Area(ground\ truth \cap predicted)}{Area(ground\ truth) + Area(predicted)} \qquad (9)$$

326
327

Table 1

Pixel classification

Real → Predicted ↓	Actual pixel ∈ OD	Actual pixel ∉ OD
System Predicted pixel ∈ OD	TP	FP
System Predicted pixel ∉ OD	FN	TN

328
329
330

Table 2

Performance metric for OD Segmentation

Measure	Description
SN	TP/(TP+FN)
SP	TN/(TN+FP)
Acc	(TP+TN)/(TP+FP+TN+FN)
PPV	TP/(TP+FP)
FDR	FP / (FP+TP)

4 Results

4.1 Optic Disc Detection

333 The optic disc detection method achieved 100% success rate in DRIVE, DIARETDB1,
334 CHASE_DB1 and Shifa databases, it achieved 99.09% in DRIONS-DB and 99.25% in the
335 Messidor database. Table 3 shows the accuracy of this method for the detection of OD. The
336 comparison of accuracy in localizing OD have been made with other methods reported in
337 literature in Table 4.

338
339

Table 3

Performance Measure of OD detection

Datasets	Images	OD detected	OD missed	Accuracy
DRIVE	40	40	0	100%
DIARETDB1	89	89	0	100%
CHASE_DB1	28	28	0	100%
DRIONS-DB	110	109	1	99.09%
Messidor	1200	1191	9	99.25%
Shifa	111	111	0	100%
ONHSD	90	90	0	100%

340
341
342

Table 4

Comparison of OD localization with other methods

Authors	Database	Accuracy
(Youssif et al. 2008)	DRIVE	98.8%
(Niemeijer et al. 2009)	Local database	99.4%
(Aquino et al. 2010)	Messidor	99%
(Welfer et al. 2010)	DRIVE	100%
	DIARETDB1	97.75%
(Lu 2011)	Messidor	98.77%
(Zubair et al. 2013)	Messidor	98.65%
(Mahfouz & Fahmy 2010)	DRIVE	100%
	DIARETDB1	97.8%
(Yu et al. 2012)	Messidor	99%
(Saleh et al. 2014)	DRIVE	100%
(Yu et al. 2015)	DRIVE	100%
	DIARETDB1	99.88%
	Messidor	99.67%
Proposed method	DRIVE	100%
	DIARETDB1	100%
	CHASEDB1	100%
	DRIONS-DB	99.09%
	Messidor	99.25%
	ONHSD	100%

343
344 Figure 5 shows the results of the OD detection in the DRIVE, DIARETDB1, Shifa,
345 CHASE_DB1 and DRIONS-DB databases. The OD detection method can correctly detect the
346 OD center even in the presence of exudates and other pathologies. Accurate detection of the
347 optic nerve head facilitates the segmentation algorithm to extract the boundary with high
348 precision.
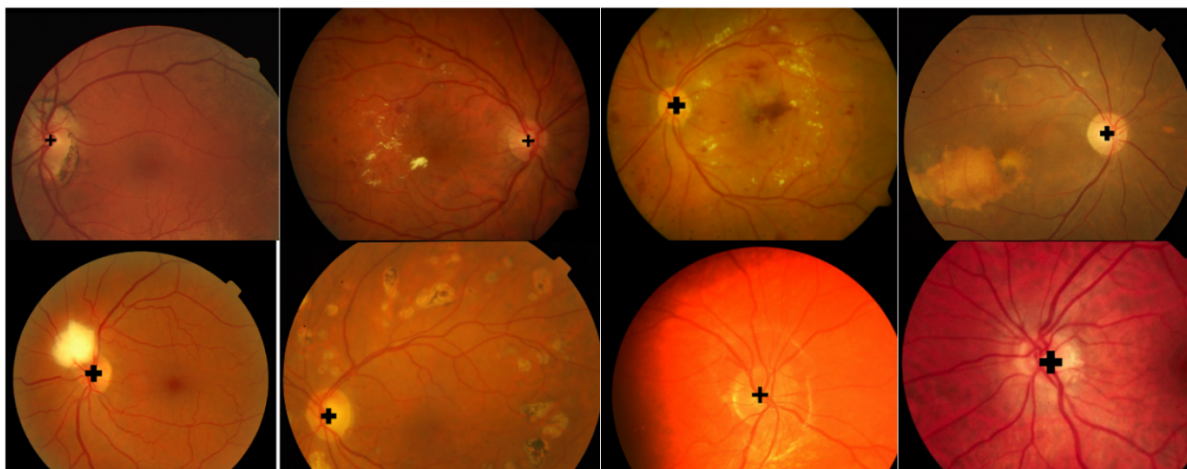
349
350 **Figure 5 OD detection results. Sorting of images in rows is according to the following order DRIVE,**
351 **DIARETDB1, Messidore, Shifa, CHASE_DB1 and DRIONS-DB**
352

353 ## 4.2   Optic Disc Segmentation

354 The pixel-wise quantitative performance metrics (which are defined in Table 2) are calculated
355 for OD segmentation, based on the comparison of automatic segmented images with the ground
356 truth reference images and are illustrated in Table 5. The methodology is quantitatively evaluated

357 by using an array of performance metrics, which to the limit of our knowledge has not been
358 previously used for evaluating OD segmentation algorithms.

359 **Table 5**
360 Performance measures of OD segmentation

Performance Measure	DRIVE	DIARET DB1	CHASE-DB1	Shifa	DRIONS-DB	Messidor	ONHSD
Acc	0.9672	0.9772	0.9579	0.9793	0.9549	0.9989	0.9967
SP	0.9966	0.9984	0.9971	0.9991	0.9966	0.9995	0.9992
SN	0.8187	0.8510	0.8313	0.8015	0.8508	0.8954	0.8857
PPV	0.8728	0.9263	0.9261	0.9493	0.9966	0.9794	0.9619
FDR	0.1271	0.0737	0.0738	0.0506	0.0810	0.020	0.038
DICE	0.8720	0.8910	0.9050	0.8763	0.9102	0.9339	0.9197
Overlap	78.6%	85.1%	83.2%	80.1%	85.1%	87.93%	86.1%
Hausdorff	0.2514	0.1915	0.3174	0.2434	0.2578	0.1627	0.2245

361
362
363 The comparison of the proposed method has been made with other available methods on the
364 basis of average sensitivity, specificity, accuracy, DICE score, overlap, positive predictive value
365 and the time taken to process a single image, as illustrated in
366
367 Table 6. Results shows that the proposed method provides promising results as compared to
368 other OD segmentation techniques in the literature. The comparison with other methods is made
369 with respect to DRIVE and DIARETDB1, DROINS-DB, Messidor and ONHSD retinal image
370 datasets.
371
372 **Table 6**
373 Comparison of OD segmentation with other methods

Performance Measures → Methods↓	Sensitivity	Specificity	Accuracy	DICE Score	Overlap %	Predictive Value	Average Time per image (in sec)
DRIVE Database							
(Sopharak et al. 2008)	0.2104	0.9993	--	--	16.88	0.9334	14.92
(Walter et al. 2002)	0.4988	0.9981	--	--	29.32	0.8653	219.6
(Seo et al. 2004)	0.5029	0.9983	--	--	31.09	0.843	7.23
(Kande et al. 2008)	0.6999	0.9888	--	--	29.66	0.5218	111.7
(Stapor et al. 2004)	0.7368	0.9920	--	--	33.42	0.6198	43.00
(Lupascu et al. 2008)	0.7768	0.9968	--	--	30.95	0.88.14	--
(Welfer et al. 2013)	0.7357	0.9982	--	--	39.40	0.8876	53.65
(Basit & Fraz 2015)	0.8921	0.9921	--	--	61.88	0.6930	--
(Morales et al. 2013)	--	--	0.9903	0.8169	--	0.8544	--
(Salazar-Gonzalez et al. 2014)	0.7512	0.9684	0.9412	--	--	--	--
Proposed Method	0.8188	0.9966	0.9672	0.8720	78.6	0.8728	59.2
DIARETDB1 Database							
(Sopharak et al. 2008)	0.4603	0.9994	--	--	29.41	0.9593	74.55
(Walter et al. 2002)	0.6569	0.9993	--	--	36.97	0.9395	308.5
(Seo et al. 2004)	0.6103	0.9987	--	--	35.32	0.8878	15.63
(Kande et al. 2008)	0.8808	0.9878	--	--	33.41	0.5448	120.5

(Stapor et al. 2004)	0.8498	0.9964	--	--	34.08	0.8034	59.72
(Lupascu et al. 2008)	0.6848	0.9969	--	--	30.95	0.8117	--
(Welfer et al. 2013)	0.6341	0.9981	--	--	39.15	0.8704	57.16
(Basit & Fraz 2015)	0.7347	0.9944	--	--	54.69	0.7049	--
(Morales et al. 2013)	--	--	0.9957	0.893	--	0.9224	--
Proposed Method	0.851	0.9984	0.9772	0.891	85.1	0.9263	40.0
DRIONS-DB							
(Walter et al. 2002)	--	--	--	0.6813	--	--	--
(Morales et al. 2013)	--	--	0.9934	0.9084	--	0.9281	--
Proposed Method	0.8508	0.9966	0.9989	0.9102	85.1	0.9794	43.2
Messidor							
(Morales et al. 2013)	--	--	0.9949	0.8950	--	0.9300	--
(Kumar et al. 2015)	--	--	--	0.8456	--	--	--
Proposed Method	0.8954	0.9995	0.9989	0.9339	87.93	0.9794	71.3
ONHSD							
(Morales et al. 2013)	--	--	0.9941	0.8867	--	0.9310	--
Proposed Method	0.8857	0.9992	0.9967	0.9197		0.9619	65.3

374
375
376 The OD segmentation results on these retinal datasets are illustrated in Figure 6. It can be
377 observed that the proposed methodology can successfully detect and segment the OD in the
378 pathological images as well as in images with non-uniform illumination and uneven background
379 pigmentation from multiple retinal image datasets.
380

381
382 **Figure 6 Examples of segmentation. Images in each row belong to separate databases as per order,**
383 **DIARETDB1, Shifa, CHASE_DB1, and DRIONS-DB. Grow Cut segmentation is represented by a green**
384 **boundary and its final approximation is represented by a black circle.**

385 ### 4.3   Robustness of Methodology
386 The robustness of proposed methodology has been evaluated on the basis of its OD localization
387 and segmentation performance on (1) the noisy images, (2) the images with illumination
388 artefacts, and (3) the images with pathological structures. The retinal images are corrupted with
389 three types of noise models typically found in biomedical images (Gaussian, Salt & Pepper, and
390 speckle noise). It can be observed in Figure 7, that OD is successfully detected and segmented
391 despite significant deterioration of the retinal images due to the addition of noise.
392
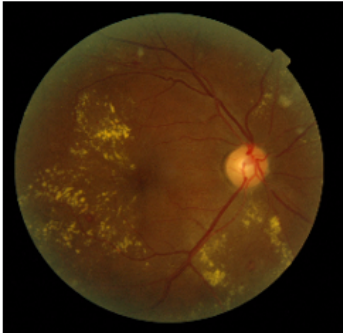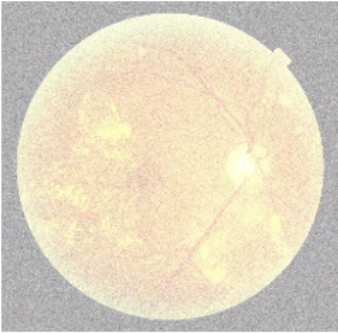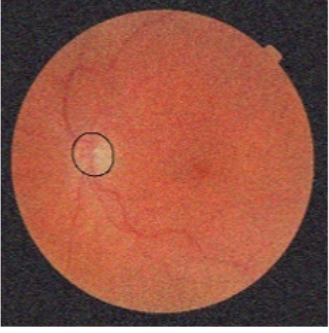
Type of noise	Original image	Noisy image	OD detection
Gaussian			
Salt & Pepper			
Speckle			

Figure 7 Performance in the noisy images

Second criteria for measuring robustness is the evaluation of against illumination which makes OD detection harder because poor illumination hide the OD in the background, as a result of which segmentation algorithms fails to extract boundary. Figure 8 shows some extreme cases of poor illumination where proposed method successfully localize and segment the OD.
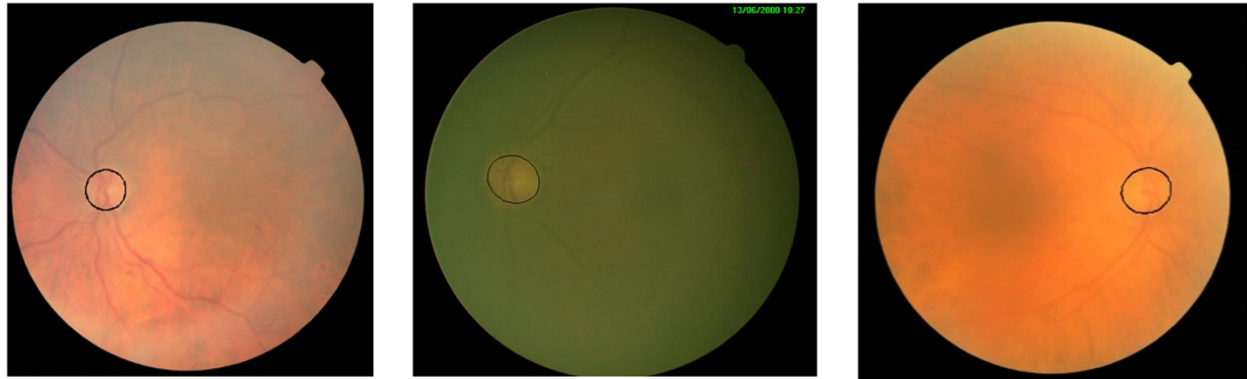
401
402 **Figure 8 Performance in the poor contrast and uneven illumination.**
403

404 Pathologies such as papillary atrophy, exudates, and lesions put a potent threat to accurate
405 segmentation of optic disc because some pathologies may appear in bright or in circular shape
406 and may result in misclassification. While others like papillary atrophy surround the OD and
407 make it difficult to segment. Figure 9 shows the result of proposed algorithm on pathologically
408 affected images.

409
410 **Figure 9 Performance in the presence of pathologies.**
411

412 Although algorithm works fine on images where segmentation is hard but in fundus imaging,
413 sometimes, there are images which are poorly focused or have imaging artefacts which make
414 segmentation a difficult task.
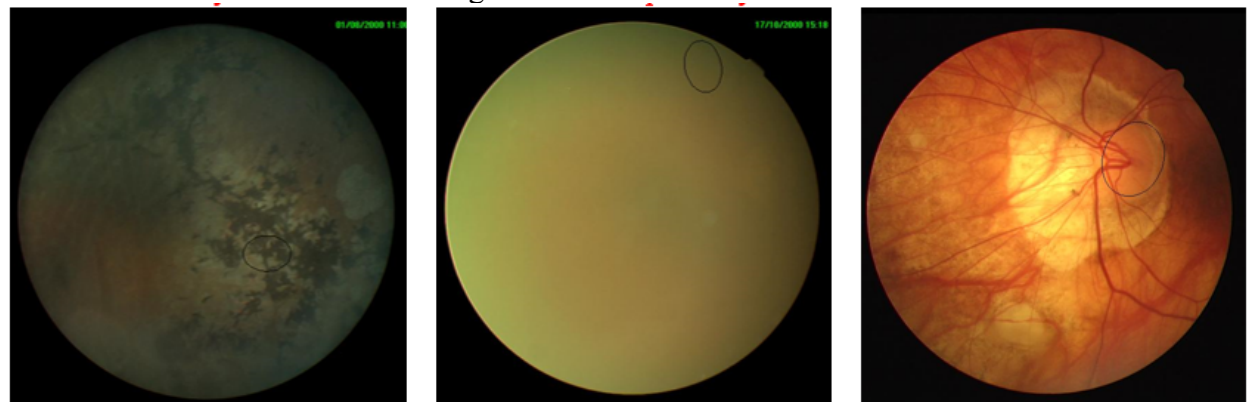
415
416 Figure 10 shows some extreme cases where method failed to extract optic disc correctly e.g. in
417 the first two images the artifacts are so strong that it almost hide out OD and leaves false

418 detection and segmentation while in the third image pathologies hide the boundary of OD and
419 leave the method to partially detect OD.
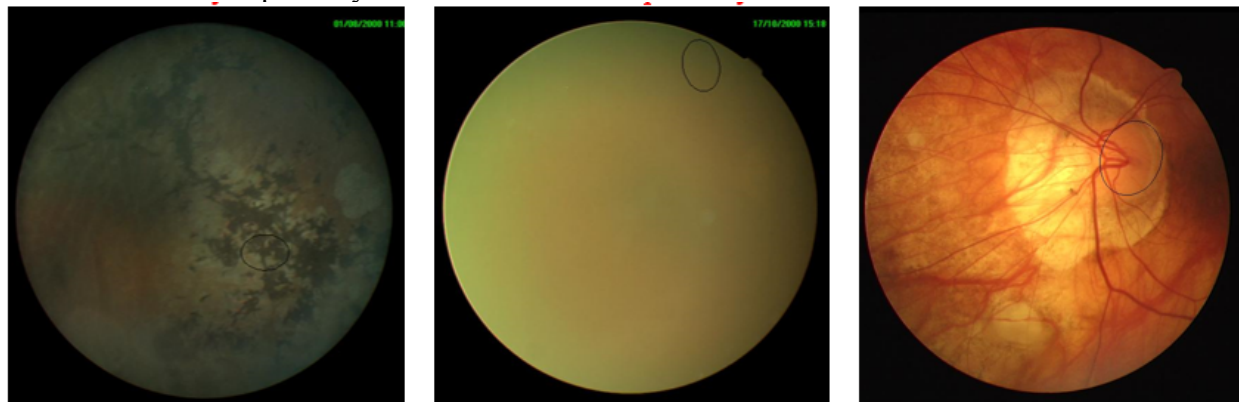
420
421 **Figure 10 Incorrect OD segmentation in difficult cases of retinal images**
422

5   Discussion and Conclusion

423
424 Optic disc segmentation is the primary step towards the development of automatic screening
425 systems. The accuracy of the segmentation method improves the correct identification of
426 pathological diseases like glaucoma. Similarly, optic disc detection is the first step towards
427 segmentation and accurate detection would lead to promising segmentation results.
428 This paper presents a new method for automatic detection and segmentation of the OD in retinal
429 images. Using morphological operations, Circular Hough Transform and Grow Cut algorithm
430 (GC). The GC algorithm has been widely used in many application areas of image segmentation,
431 but has not been applied within the framework of retinal image analysis. To the limit of our
432 knowledge, the GC algorithm has been utilized for the first time in segmenting the OD in retinal
433 images. The method is evaluated on six retinal image datasets exhibiting different morphological
434 characteristics. Experimental evaluation shows that this method is computationally fast in
435 processing, robust to the variation in image contrast and illumination, works well in pathological
436 retinal images and comparable with state-of-the-art methodologies in terms of quantitative
437 performance metrics. The methodology offers 100% OD detection rate in DRIVE, DIARETDB1,
438 CHASE_DB1, ONHSD, and Shifa databases, and 99.09% success rate in DRIONS-DB1. For the
439 OD segmentation we use the detected OD center point as the seed for the Grow Cut algorithm,
440 which then iteratively searches for neighbors of initial seeds and expands the region based on the
441 label and strength of each pixel. The proposed method is able to segment the OD with a better
442 overlap ratio, as compared to other methods available in the literature. We achieved 78.6%,
443 85.1%, 83.2%, 80.1%, 85.1%, 87.93%, and 86.1% in DRIVE, DIARETDB1, CHASE_DB1,
444 Shifa, DRIONS-DB1, Messidor, and ONHSD databases respectively. The results of the
445 presented algorithm can be seen online at http://vision.seecs.edu.pk/od/.
446 OD segmentation results clearly depict the ability of proposed method to segment, even with
447 illumination artifacts when the OD boundary is not clear and in the presence of pathologies like
448 papillary atrophy, which may increase the chances of false positives. The robustness of proposed
449 methodology has been evaluated on the basis of its OD localization and segmentation
450 performance on (1) the noisy images, (2) the images with illumination artefacts, and (3) the
451 images with pathological structures. For evaluation purpose, the retinal images have been
452 corrupted with three types of noises generally found in biomedical images, the Gaussian, Salt &

453 pepper, and Speckle noise. The methodology successfully segment the OD despite significant
454 deterioration of the retinal images. Moreover, the algorithms performs well on the images with
455 uneven illumination and the pathological structures.
456 The work is aimed at contributing to the development of an automatic system for glaucoma
457 detection that is currently under development. Although other published solutions can be used,
458 this work presents higher accuracy, robustness and is tolerant to a vast variety of images which
459 make it suitable for integration with a glaucoma detection system.
460 We have already developed a fully automated software system named QUARTZ (Fraz et al.
461 2015), which can extract a number of quantifiable measures from retinal vessel morphology.
462 These measures are analyzed/studied by epidemiologists and other medical/statistical experts in
463 order to evaluate the association of retinal vessel abnormalities with other systemic diseases. In
464 future, we aim to enhance the aforementioned software system and extend its functionality by
465 incorporating a module for early detection of glaucoma in large population based screening
466 programs. The proposed method for reliable segmentation of OD can be seen as a first step
467 towards the development of a glaucoma detection module.

Acknowledgment

469 The Authors would like to thank teams of DRIVE, DIARETDB1, CHASE_DB1, DRIONS-DB,
470 Messidor and ONHSD for maintaining and keeping these databases active and making them
471 easily accessible for researchers to carry out retinal image analysis research. Furthermore, we
472 would also thank the experts from the Armed Forces Institute of Ophthalmology, Rawalpindi,
473 Pakistan for taking the time to establish the ground truth images.

References

475 2004. DRIVE: Digital Retinal Images for Vessel Extraction.
476 Abdullah M, and Fraz MM. 2015. Application of grow cut algorithm for localization and extraction of
477   optic disc in retinal images. 2015 12th International Conference on High-capacity Optical
478   Networks and Enabling/Emerging Technologies (HONET): IEEE. p 1-5.
479 Abramoff MD, Garvin MK, and Sonka M. 2010. Retinal Imaging and Image Analysis. *Biomedical*
480   *Engineering, IEEE Reviews in* 3:169-208. 10.1109/rbme.2010.2084567
481 Aquino A, Gegúndez-Arias ME, and Marín D. 2010. Detecting the optic disc boundary in digital fundus
482   images using morphological, edge detection, and feature extraction techniques. *Medical*
483   *Imaging, IEEE Transactions on* 29:1860-1869.
484 Basit A, and Fraz MM. 2015. Optic disc detection and boundary extraction in retinal images. *Applied*
485   *Optics* 54:3440-3447. 10.1364/ao.54.003440
486 Carmona EJ, Rincón M, García-Feijoó J, and Martínez-de-la-Casa JM. 2008. Identification of the optic
487   nerve head with genetic algorithms. *Artificial Intelligence in Medicine* 43:243-259.
488 Cheng J, Liu J, Xu Y, Yin F, Wong DWK, Tan N-M, Tao D, Cheng C-Y, Aung T, and Wong TY. 2013.
489   Superpixel classification based optic disc and optic cup segmentation for glaucoma screening.
490   *Medical Imaging, IEEE Transactions on* 32:1019-1032.
491 Dashtbozorg B, Mendonça AM, and Campilho A. 2015. Optic disc segmentation using the sliding band
492   filter. *Computers in biology and medicine* 56:1-12.
493 Decenciere E, Zhang X, Cazuguel G, Laÿ B, Cochener B, Trone C, Gain P, Ordónez-Varela J-R, Massin P,
494   and Erginay A. 2014. Feedback on a publicly distributed image database: the MESSIDOR
495   database. *Image Analysis and Stereology*:231-234.

496   Federation ID. 2013. International Diabetic Federation Atlas; Chapter 2 The Gobal Burden. *Available at*
497   *http://www.idf.org/sites/default/files/EN_6E_Ch2_the_Global_Burden.pdf* (accessed 3
498   December 2015).
499   Foracchia M, Grisan E, and Ruggeri A. 2005. Luminosity and contrast normalization in retinal images.
500   *Medical image analysis* 9:179-190. 10.1016/j.media.2004.07.001
501   Fraz MM, Basit A, and Barman SA. 2012a. Application of Morphological Bit Planes in Retinal Blood Vessel
502   Extraction. *Journal of Digital Imaging*:1-13. 10.1007/s10278-012-9513-3
503   Fraz MM, Remagnino P, Hoppe A, Uyyanonvara B, Rudnicka AR, Owen CG, and Barman SA. 2012b. Blood
504   vessel segmentation methodologies in retinal images – A survey. *Computer methods and*
505   *programs in biomedicine* 108:407-433.
506   Fraz MM, Remagnino P, Hoppe A, Uyyanonvara B, Rudnicka AR, Owen CG, and Barman SA. 2012c. An
507   Ensemble Classification-Based Approach Applied to Retinal Blood Vessel Segmentation.
508   *Biomedical Engineering, IEEE Transactions on* 59:2538-2548. 10.1109/TBME.2012.2205687
509   Fraz MM, Rudnicka A, Owen C, and Barman S. 2014. Delineation of blood vessels in pediatric retinal
510   images using decision trees-based ensemble classification. *International Journal of Computer*
511   *Assisted Radiology and Surgery* 9:795-811. 10.1007/s11548-013-0965-9
512   Fraz MM, Welikala RA, Rudnicka AR, Owen CG, Strachan DP, and Barman SA. 2015. QUARTZ:
513   Quantitative Analysis of Retinal Vessel Topology and size – An automated system for
514   quantification of retinal vessels morphology. *Expert Systems with Applications* 42:7221-7234.
515   http://dx.doi.org/10.1016/j.eswa.2015.05.022
516   Haleem MS, Han L, van Hemert J, and Li B. 2013. Automatic extraction of retinal features from colour
517   retinal images for glaucoma diagnosis: A review. *Computerized Medical Imaging and Graphics*
518   37:581-596.
519   Hoover A, and Goldbaum M. 2003. Locating the optic nerve in a retinal image using the fuzzy
520   convergence of the blood vessels. *Medical Imaging, IEEE Transactions on* 22:951-958.
521   Hough PV. 1962. Method and means for recognizing complex patterns.
522   Hsiao H-K, Liu C-C, Yu C-Y, Kuo S-W, and Yu S-S. 2012. A novel optic disc detection scheme on retinal
523   images. *Expert Systems with Applications* 39:10600-10606.
524   Illingworth J, and Kittler J. 1987. The Adaptive Hough Transform. *Pattern Analysis and Machine*
525   *Intelligence, IEEE Transactions on* PAMI-9:690-698. 10.1109/tpami.1987.4767964
526   Jack J. Kanski, and Brad Bowling. 2015. *Clinical Ophthalmology: A Systematic Approach*. London: Elsevier
527   Health Sciences (UK).
528   Joshi GD, Sivaswamy J, and Krishnadas S. 2011. Optic disk and cup segmentation from monocular color
529   retinal images for glaucoma assessment. *Medical Imaging, IEEE Transactions on* 30:1192-1205.
530   Kande GB, Subbaiah PV, and Savithri TS. 2008. Segmentation of exudates and optic disk in retinal
531   images. Computer Vision, Graphics & Image Processing, 2008 ICVGIP'08 Sixth Indian Conference
532   on: IEEE. p 535-542.
533   Kauppi T, Kalesnykiene V, Kamarainen J-K, Lensu L, Sorri I, Raninen A, Voutilainen R, Pietilä J, Kälviäinen
534   H, and Uusitalo H. 2007. DIARETDB1 diabetic retinopathy database and evaluation protocol.
535   Medical Image Understanding and Analysis (MIUA2007). Aberystwyth, Wales, UK. p 61-65.
536   Kumar JH, Pediredla AK, and Seelamantula CS. 2015. Active discs for automated optic disc segmentation.
537   2015 IEEE Global Conference on Signal and Information Processing (GlobalSIP): IEEE. p 225-229.
538   Lowell J, Hunter A, Steel D, Basu A, Ryder R, Fletcher E, and Kennedy L. 2004. Optic nerve head
539   segmentation. *Medical Imaging, IEEE Transactions on* 23:256-264.
540   Lu S. 2011. Accurate and efficient optic disc detection and segmentation by a circular transformation.
541   *Medical Imaging, IEEE Transactions on* 30:2126-2133.

542   Lupascu CA, Tegolo D, and Rosa LD. 2008. Automated detection of optic disc location in retinal images.
543   Computer-Based Medical Systems, 2008 CBMS'08 21st IEEE International Symposium on: IEEE. p
544   17-22.
545   Mahfouz AE, and Fahmy AS. 2010. Fast localization of the optic disc using projection of image features.
546   *Image Processing, IEEE Transactions on* 19:3285-3289.
547   Marin D, Gegundez-Arias ME, Suero A, and Bravo JM. 2015. Obtaining optic disc center and pixel region
548   by automatic thresholding methods on morphologically processed fundus images. *Computer*
549   *methods and programs in biomedicine* 118:173-185.
550   Mendonca AM, Sousa A, Mendonca L, and Campilho A. 2013. Automatic localization of the optic disc by
551   combining vascular and intensity information. *Computerized Medical Imaging and Graphics*
552   37:409-417.
553   Mittapalli PS, and Kande GB. 2016. Segmentation of optic disk and optic cup from digital fundus images
554   for the assessment of glaucoma. *Biomedical Signal Processing and Control* 24:34-46.
555   Morales S, Naranjo V, Angulo J, and Alcañiz M. 2013. Automatic detection of optic disc based on PCA
556   and mathematical morphology. *Medical Imaging, IEEE Transactions on* 32:786-796.
557   Niemeijer M, Abràmoff MD, and Van Ginneken B. 2009. Fast detection of the optic disc and fovea in
558   color fundus photographs. *Medical image analysis* 13:859-870.
559   Pourreza-Shahri R, Tavakoli M, and Kehtarnavaz N. 2014. Computationally efficient optic nerve head
560   detection in retinal fundus images. *Biomedical Signal Processing and Control* 11:63-73.
561   Salazar-Gonzalez A, Kaba D, Li Y, and Liu X. 2014. Segmentation of the Blood Vessels and Optic Disk in
562   Retinal Images. *Biomedical and Health Informatics, IEEE Journal of* 18:1874-1886.
563   Saleh MD, Salih N, Eswaran C, and Abdullah J. 2014. Automated segmentation of optic disc in fundus
564   images. Signal Processing & its Applications (CSPA), 2014 IEEE 10th International Colloquium on:
565   IEEE. p 145-150.
566   Seo J, Kim K, Kim J, Park K, and Chung H. 2004. Measurement of ocular torsion using digital fundus
567   image. Engineering in Medicine and Biology Society, 2004 IEMBS'04 26th Annual International
568   Conference of the IEEE: IEEE. p 1711-1713.
569   Sopharak A, Uyyanonvara B, Barman S, and Williamson TH. 2008. Automatic detection of diabetic
570   retinopathy exudates from non-dilated retinal images using mathematical morphology methods.
571   *Computerized Medical Imaging and Graphics* 32:720-727.
572   http://dx.doi.org/10.1016/j.compmedimag.2008.08.009
573   Stapor K, Świtonski A, Chrastek R, and Michelson G. 2004. Segmentation of fundus eye images using
574   methods of mathematical morphology for glaucoma diagnosis. *Computational Science-ICCS*
575   *2004*: Springer, 41-48.
576   Toffoli T, and Margolus N. 1987. *Cellular automata machines: a new environment for modeling*: MIT
577   Press.
578   Vázquez SG, Cancela B, Barreira N, Penedo MG, Rodríguez-Blanco M, Pena Seijo M, Tuero GC, Barceló
579   MA, and Saez M. 2013. Improving retinal artery and vein classification by means of a minimal
580   path approach. *Machine Vision and Applications* 24:919-930. 10.1007/s00138-012-0442-4
581   Vezhnevets V, and Konouchine V. 2005. GrowCut: Interactive multi-label ND image segmentation by
582   cellular automata. proc of Graphicon: Citeseer. p 150-156.
583   Walter T, Klein J-C, Massin P, and Erginay A. 2002. A contribution of image processing to the diagnosis of
584   diabetic retinopathy-detection of exudates in color fundus images of the human retina. *Medical*
585   *Imaging, IEEE Transactions on* 21:1236-1243.
586   Weinreb RN, Aung T, and Medeiros FA. 2014. The pathophysiology and treatment of glaucoma: A
587   review. *JAMA* 311:1901-1911. 10.1001/jama.2014.3192

588 Welfer D, Scharcanski J, Kitamura CM, Dal Pizzol MM, Ludwig LW, and Marinho DR. 2010. Segmentation
589   of the optic disk in color eye fundus images using an adaptive morphological approach.
590   *Computers in biology and medicine* 40:124-137.
591 Welfer D, Scharcanski J, and Marinho DR. 2013. A morphologic two-stage approach for automated optic
592   disk detection in color eye fundus images. *Pattern Recognition Letters* 34:476-485.
593 Youssif AA-HA-R, Ghalwash AZ, and Ghoneim AASA-R. 2008. Optic disc detection from normalized digital
594   fundus images by means of a vessels' direction matched filter. *Medical Imaging, IEEE*
595   *Transactions on* 27:11-18.
596 Yu H, Barriga ES, Agurto C, Echegaray S, Pattichis MS, Bauman W, and Soliz P. 2012. Fast localization and
597   segmentation of optic disk in retinal images using directional matched filtering and level sets.
598   *Information Technology in Biomedicine, IEEE Transactions on* 16:644-657.
599 Yu T, Ma Y, and Li W. 2015. Automatic localization and segmentation of optic disc in fundus image using
600   morphology and level set. Medical Information and Communication Technology (ISMICT), 2015
601   9th International Symposium on: IEEE. p 195-199.
602 Zubair M, Yamin A, and Khan SA. 2013. Automated detection of Optic Disc for the analysis of retina using
603   color fundus image. Imaging Systems and Techniques (IST), 2013 IEEE International Conference
604   on: IEEE. p 239-242.
605
606